ADVANCED FUNCTIONAL MATERIALS
www.afm-journal.de

Polymer Nanocomposites Containing Carbon Nanofibers as Soft Printable Sensors Exhibiting Strain-Reversible Piezoresistivity

*Hatice A. K. Toprakci, Saral K. Kalanadhabhatla, Richard J. Spontak, and Tushar K. Ghosh**

Designed as flexible and extendable conductive print media for pervasive computing as strain sensors, nanocomposites composed of a plasticized thermoplastic or a cross-linked elastomer and containing carbon nanofibers at concentrations just above the percolation threshold are observed to exhibit a uniquely strain-reversible piezoresistive response upon application of quasi-static tensile strain. At small strain levels, the electrical resistance of these nanocomposites reduces with increasing strain, indicative of negative piezoresistivity. Beyond a critical strain, however, the resistance reverses and increases with increasing strain, revealing the existence of a negative-to-positive piezoresistivity transition that is fully strain-reversible and repeatable upon strain cycling. These characteristics imply that the nanocomposite morphologies are highly stable with little evidence of mechanical hysteresis. The mechanism underlying this transition is attributed to reorientation of high-aspect-ratio nanofibers (initially homogeneously dispersed) at low strains, followed by separation at high strains. While deposition of these nanocomposites as robust print coatings on textile fabric alters the percolation threshold, strain-reversible piezoresistivity is retained, confirming that they are suitable as printable strain sensors.

1. Introduction

Simultaneous growth of and continued interest in portable electronic devices and responsive soft materials have synergistically heralded a new generation of functional products.[1–4] Of these, electronic textiles ("e-textiles") now constitute a significant part of the evolving paradigm referred to as pervasive computing. Systems/devices in this category are generated by incorporating electronic capabilities (e.g., microprocessors) into flexible textiles for various sensory applications. Conventional integration of such functionality can be external, in which semiconductor-based devices/modules are embedded into fabrics, or integral, wherein the constituents (e.g., fibers or yarns) of a textile product are directly fashioned into electrical devices.[5] One viable means by which to introduce such functionality relies on the application of thin conductive coatings on fabric surfaces in the form of printed layers. A wide variety of commercial coating technologies, ranging from inkjet to screen printing, is currently available for this purpose.[6,7] Most studies of conductive coatings have focused on the use of conducting polymers, such as polypyrrole.[8–10] The nontrivial drawback of such polymers, however, is that they frequently require complicated and expensive processing routes and lack environmental stability. In contrast, appropriately printed fabric coatings consisting of conductive polymer nanocomposites (CPNs), which contain conductive fillers that can vary in both size and shape, are generally more straightforward and cost-effective to apply, especially over large areas, than conductive polymers. Even though they may eventually suffer from interfacial debonding upon repeated mechanical cycling, additional benefits of elastomeric CPNs include high extensibility, as well as composition-tunable conductivity and fabric-compatible mechanical properties.

To ensure optimal mechanical behavior of the printed layer and avoid added material and processing expenses, CPNs should be prepared with conductive fillers that inherently possess a low volume-fraction percolation threshold (φ^*), which corresponds to the filler concentration signifying the formation

Dr. H. A. K. Toprakci, Dr. S. K. Kalanadhabhatla, Prof. T. K. Ghosh
Department of Textile Engineering Chemistry & Science and Fiber & Polymer Science Program
North Carolina State University
Raleigh, NC 27695, USA
E-mail: tghosh@ncsu.edu
Dr. S. K. Kalanadhabhatla, Prof. R. J. Spontak
Department of Materials Science & Engineering
North Carolina State University
Raleigh, NC 27695, USA
Prof. R. J. Spontak
Department of Chemical & Biomolecular Engineering
North Carolina State University
Raleigh, NC 27695, USA
Prof. R. J. Spontak
Department of Chemical Engineering
Norwegian University of Science & Technology
N-7491 Trondheim, Norway

DOI: 10.1002/adfm.201300034

of a continuous electrically conductive pathway (or network) within the polymer matrix.[11] For this reason, nanoscale carbonaceous fillers such as carbon nanotubes (CNTs), carbon black (CB), graphene, and carbon nanofibers (CNFs) are ideally suited for inclusion in CPNs due to their excellent and stable electromechanical properties and large surface-to-volume ratio.[12] Their correspondingly high surface energy likewise facilitates surface functionalization[13] and can promote good dispersion and strong matrix-filler association in organic polymers.[14,15] Here, we turn our attention to high-aspect-ratio (fiber-like) fillers such as CNTs, which tend to possess high conductivity levels (10^4–10^5 S cm^{-1})[16] and low values of φ^* (less than 0.1–6.2 vol%),[17,18] and CNFs, for which φ^* typically ranges from 0.5 to 2.0 vol%, depending on processing and the characteristics of the CNFs.[19–21] Of these, CNFs are of particular interest because of their facile and uniform dispersability in organic media, as well as their low cost relative to CNTs. Despite the fact that their conduction levels and electron transduction properties are inferior to those of metals and semiconductors, CPNs containing a carbonaceous nanofiller such as CNFs can be designed to adhere strongly to flexible textile substrates, thereby making them suitable as conductive print media for e-textiles.

Although emergent textile applications, such as photovoltaic cells[22] and organic transistors,[23] are expected to benefit from the design of CPNs, examples of CPN-based textile systems already developed include strain sensors for health monitoring[24] and biomechanics.[25] Physiological strain sensing can be used to continuously record bodily functions such as respiration and cardiovascular activity[26] in real time. Such sensors generally operate on the principle of piezoresistance, which relates the resistivity of a sensor to a change in strain state. Piezoresistive behavior is typically encountered in CPNs containing a variety of carbonaceous or metallic nano- or microscale objects. Contemporary research efforts aimed at improving strain sensors strive to develop high-sensitivity systems with superior signal integrity, which can be compromised by the intrinsic viscoelastic behavior of thermoplastics. For instance, creep contributes to inconsistencies in resistance and sensitivity[27] by adversely affecting the reproducibility of the resistance-strain response upon strain cycling. To overcome complications due to viscous losses, Cochrane et al.[28] have developed textile strain sensors with CPNs generated from a CB-reinforced thermoplastic elastomer, which was printed on nylon. They find that, at 26 vol% CB, the resistance of their CPN increases monotonically with increasing strain, which is referred to as positive piezoresistance. Positive piezoresistivity is generally observed when a CPN is subjected to in-plane uniaxial tensile strain. Mattmann et al.[29] report that a similarly designed CPN containing 50 wt% CB consistently displays linear and positive piezoresistance with minimum hysteresis when repeatedly cycled to 100% strain. Using silicone elastomers, de Rossi and co-workers[30] have shown that their CPNs, exhibiting nonlinear positive piezore-sistance, can be used to record posture, gestures and respiration.

2. Results and Discussion

In this study, we report on the development of lightweight, conformable sensory materials based on two different polymeric systems that can be used for printing on textile substrates. The first, generically termed "plastisol," is a multicomponent material commonly used for textile printing and derived from plasticized poly(vinyl chloride) (pPVC) in the presence of other additives that promote stability and adhesion to textile substrates. The second is cross-linked poly(dimethylsiloxane) (PDMS), which is a highly elastic and extensible elastomer with silica reinforcement. It generally adheres well to other polymers, and it is both thermally stable and chemically inert. Because of their property attributes, i.e., low cost, facile processing and long-term durability, these two materials are well-suited as print media for textiles. Here, we report that CPNs produced from these polymeric systems loaded with CNFs are capable of systematically exhibiting reversible positive or negative piezoresistance depending on the strain level imposed, and we further demonstrate that screen-printing can be used in straightforward fashion to fabricate large-area, flexible strain sensors by depositing a strain-reversible piezoresistive print layer of each CPN on a commercial textile fabric.

2.1. Static Percolation Behavior

The electrical properties of the CPNs produced here are provided in **Figure 1**, wherein resistivity (ρ) is presented as a function of CNF volume fraction (φ) for pPVC- and PDMS-based films (Figure 1a,c, respectively). Both systems initially exhibit high resistivity levels, with PDMS being more resistive (by over four orders of magnitude) than pPVC. Upon addition of CNFs, the two series eventually reach φ^*, at which point the resistivity drops precipitously (by ca. nine orders of magnitude for PDMS) as the CPNs become conductive due to quantum mechanical tunneling. In Figure 1a, the position of φ^* is sensitive to the composition of the pPVC matrix, shifting to higher values as the concentration of plasticizer (dioctyl sebacate, DOS) is increased and the CNFs are more fully wetted as the pPVC matrix is softened. At values of $\varphi > \varphi^*$, $\rho \propto (\Phi - \Phi*)^{-}\beta$, where β is the critical exponent. Values of φ^* and β extracted from this relationship are listed in **Table 1** for both CPN systems; these reveal that β decreases (due to enhanced surface wetting and dispersion of the CNFs), while φ^* increases (due to greater separation of the CNFs because of the lower density of DOS relative to PVC) with increasing DOS content in the pPVC systems. According to percolation theory,[31] β adopts a universal value of 2 for ideal three-dimensional networks. Non-universal behavior due to a heterogeneous network and variable charge carrier densities is, however, observed here, as well as for a variety of CPNs,[32–37] and predicted by models that consider effects such as random voids,[38] tunneling-percolation,[39] and shear rate.[40] Included for comparison in the insets of Figures 1a and c are ρ values measured from CPN layers deposited by screen printing on a commercial knitted fabric composed of 92 wt% nylon and 8 wt% Spandex. In both cases, ρ measured from the printed fabrics is substantially lower (by over six orders of magnitude in some cases) than that of freestanding films. Depending on CNF content, the difference in measured ρ values between films and printed layers of pPVC-based CPNs tends to be more pronounced compared to PDMS-containing CPNs (for which the maximum difference in ρ between films and their print

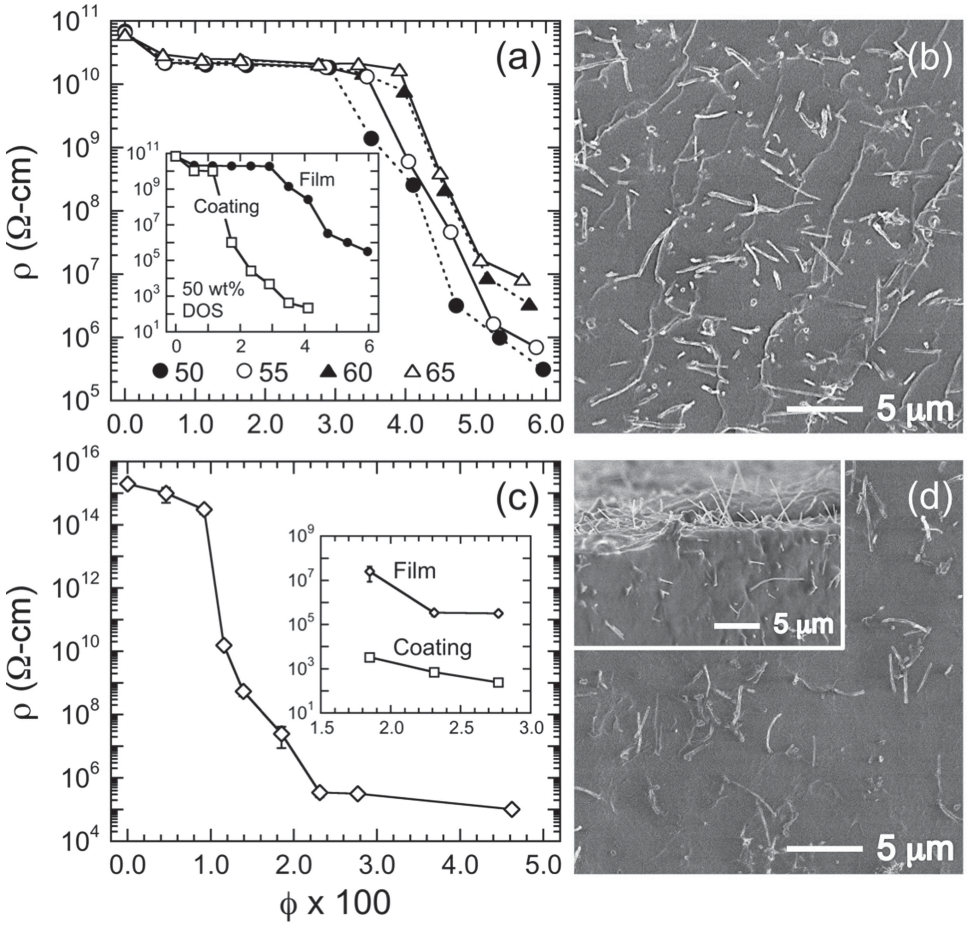

Figure 1. Variation of electrical resistivity (ρ) with CNF volume-fraction concentration (φ) for CPNs composed of: a) pPVC varying in DOS concentration (in wt%, labeled in the key), and c) PDMS. The insets show ρ as a function of φ for freestanding films and printed fabric coatings (labeled). Cross-sectional SEM images of: b) pPVC- and d) PDMS-based CPN films; an edge-view image is included in the inset of (d).

analogs is ca. four orders of magnitude). While the reason for these differences can be explained in terms of coating morphology (discussed later), the initially isotropic distribution of CNFs in films of both systems is evident in the cross-sectional scanning electron microscopy (SEM) images included in Figure 1b (pPVC with 50 wt% DOS and 8 wt% CNF) and Figure 1d (PDMS with 4 wt% CNF). An edge view of a fracture surface is included in the inset of Figure 1d that clearly shows CNFs extending from the PDMS matrix.

Table 1. Percolation characteristics of the CPN films examined in this study.

Polymer	DOS concentration [wt%]	$\varphi^* \times 100$	β
PVC	50	2.99	4.83
	55	3.35	3.05
	60	3.80	3.18
	65	3.88	1.87
PDMS		0.85	6.63

2.2. Cyclical Piezoresistive Behavior

To elucidate the dependence of electrical behavior on applied strain for the CPNs generated here, we have evaluated the simultaneous strain response and parallel resistance of CPNs varying in composition and subjected to at least ten uniaxial loading and unloading cycles ranging in strain amplitude. The continuous DC properties thus measured from select CPNs in both polymer series are shown in **Figure 2**. In each panel, electrical resistance is provided as a function of strain for the first and tenth strain cycles, and the corresponding ten-cycle dynamic response is included in each inset. Several general features of this figure montage warrant discussion. First, the results given in the insets confirm that the electrical properties of the CPNs examined here do not vary appreciably with strain cycling over time, implying that the CNF morphology is robust and exhibits little mechanical hysteresis. (This anticipated behavior is evident after 42 strain cycles in the data provided for a pPVC-based CPN in the Supporting Information.) In each single cycle, the resistance is observed to exhibit three different stages of development. After a small plateau or increase due to hysteresis (visible in the single cycles in Figure 2a–c),

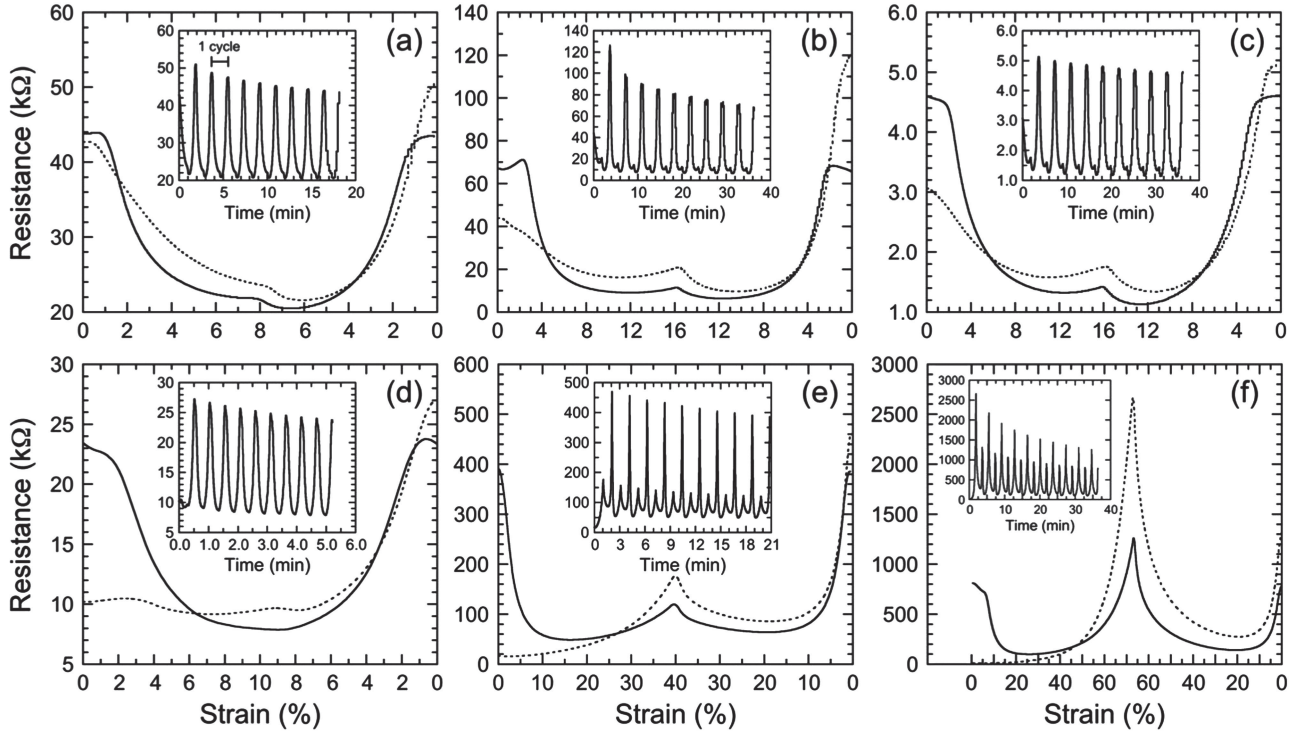

Figure 2. Dependence of the first- and tenth-cycle electrical resistance (dotted and solid lines, respectively) on strain for pPVC-based CPNs containing different CNF concentrations and subjected to two maximum strain levels (in wt%/%): a) 8/8, b) 8/16, and c) 9/16; and PDMS-based CPNs containing 4 wt% CNF at three maximum strain amplitudes (in%): d) 10, e) 40, and f) 70. The inset in each panel shows the full ten-cycle response of the electrical resistance as a function of measurement time.

the resistance measured at small strain levels consistently decreases linearly with increasing strain (negative piezoresistivity) in Stage I. As the strain is increased further (Stage II), the electrical resistance reduces more slowly and eventually exhibits a minimum at a critical piezoresistive transition strain (ε_c). At strain levels beyond ε_c in Stage III, the resistance increases with increasing strain (positive piezoresistivity) until the strain direction is reversed. These data indicate that the transition observed is strain-reversible, that is, the transition occurs upon both loading and unloading. In Figure 2a–c, the maximum strain of and CNF concentration in pPVC-based CPNs (with 50 wt% DOS) are varied from 8 to 16% and 8 to 9 wt%, respectively, to illustrate the effects of composition and strain amplitude on strain-dependent resistance, whereas the strain amplitude is increased further (from 10 to 70%) for a PDMS-containing CPN with 4 wt% CNF in Figures 2 d–f. Due to its elastomeric nature, PDMS can withstand significantly larger strain levels than pPVC.

While similarly strain-reversible piezoresistive behavior has been previously reported for PDMS/graphene[41] and polyurethane/CNT[42] nanocomposites, the results displayed in **Figure 3** further demonstrate that ε_c changes with cycle number for two PDMS-based CPNs varying in CNF content and subjected to different strain amplitudes. In all cases, ε_c consistently escalates from the first cycle to the second, but remains relatively constant thereafter, and the magnitude of the initial increase in ε_c tends to likewise grow with increasing strain amplitude. The same general behavior is observed (albeit to a less pronounced extent) for pPVC-based CPNs, and values of their first- and tenth-cycle ε_c are provided at different compositions in **Table 2**. The stage-wise piezoresistive response observed in the present CNF systems (but not seen in analogous CB-modified CPNs

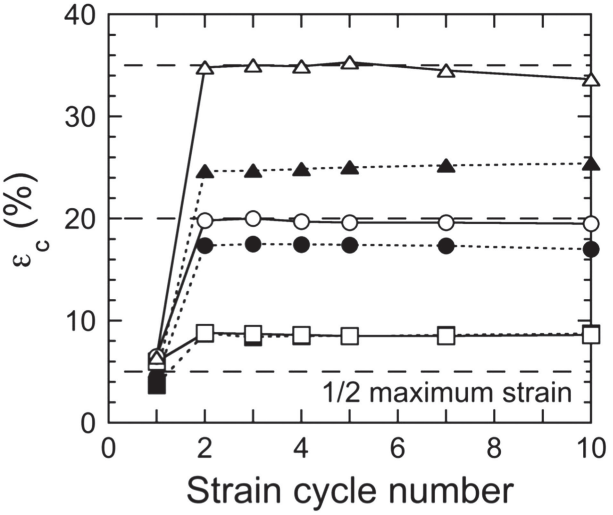

Figure 3. The critical transition strain (ε_c) presented as a function of cycle number for PDMS-based CPN films varying in CNF concentration and strain amplitude (in wt%/%): 4/10 (■), 4/40 (●), 4/70 (▲), 5/10 (□), 5/40 (○), and 5/70 (△). The dotted and solid lines serve to connect the data for CPNs with 4 and 5 wt% CNF, respectively, and the dashed horizontal lines identify the strain levels corresponding to half the maximum applied strain. Values of ε_c are listed in Table 1 for PDMS- and pPVC-containing CPNs.

Table 2. Gauge factors determined for the CPN films under investigation.[a)]

Polymer	CNF concentration [wt%]	Maximum strain [%]	ε_c		K
			1st cycle	10th cycle	
PVC[b)]	8	12	10.9	11.4	–20.4
	8	16	11.7	12.7	–42.6
	9	12	11.1	11.8	–19.6
	9	16	11.9	14.1	–22.5
PDMS	4	10	3.7	8.7	–13.8
	4	40	4.5	17.0	–14.6
	4	70	4.6	25.4	–14.8
	5	10	6.0	8.6	–7.9
	5	40	6.5	19.5	–8.6
	5	70	6.4	33.6	–8.8

[a)]While volume-fraction concentrations are used in the calculation of φ^* and β, CNF concentrations are reported here and in the text on a weight basis because they are more practical from an experimental standpoint; [b)]The pPVC formulations contained 50 wt% DOS.

that only exhibit positive piezoresistivity[43]) can be attributed to the high aspect ratio of the CNFs and the corresponding strain-induced changes in the percolation network. More specifically, two changes in CPN morphology that result from an applied strain must be considered: i) rotation, as well as straightening, of individual CNFs, and, ii) translation of high-aspect-ratio CNFs, which dictates the efficacy of conducting pathways, as illustrated in **Figure 4**. At small strains ($\varepsilon < \varepsilon_c$ in Figure 4b), the mean interparticle separation (i.e., the shortest distance between CNFs) decreases due to rotation of CNFs that are out of plane, leading to improved in-plane alignment and greater electrical conductivity (negative piezoresistivity). At much higher strains ($\varepsilon > \varepsilon_c$ in Figure 4d), however, the in-plane interparticle separation of aligned CNFs increases so that conductive pathways are broken and the CPN consequently becomes increasingly more resistive (positive piezoresistivity). At $\varepsilon = \varepsilon_c$ (Figure 4c) these two competing considerations are balanced. While a number of previous studies[44–48] have demonstrated that maximum conductivity is achieved with slightly aligned CNTs in thermoplastic-based nanocomposites, the present study establishes the effect of applied dynamic strain on the electrical (or piezoresistive) behavior of soft films and printed coatings derived from cross-linked elastomers and plasticized thermoplastics.

The strain-induced interparticle separation ($S\varepsilon$) for a composite material containing spherical particles and subjected to uniaxial strain can be estimated[49] from a plane-strain transformation of the form $S\varepsilon/S_0 = 1 + \varepsilon_x(\cos^2\theta - \upsilon_{xy}\sin^2\theta) + \gamma_{xy}\sin\theta\cos\theta$, where S_0 is the unstrained interparticle separation, θ represents the average orientation angle between the direction of applied strain and the electron tunneling path, υ_{xy} is Poisson's ratio, and γ_{xy} denotes the applied shear strain. In the absence of shear strain, this relationship is used to illustrate the dependence of $S\varepsilon$ on θ for a system with $\upsilon_{xy} = 0.4$ at applied strains ranging from 50 to 200% in Figure 4e. Under these conditions, $S\varepsilon/S_0$ is predicted to decrease (below unity) over a strain-independent interval, but increase outside this interval. While these results are strictly valid for isotropic materials in in-plane strain, they do help in understanding changes in $S\varepsilon$ that accompany strain in composite systems containing high-aspect-ratio fibers. Included in Figure 4f are several conceptual scenarios wherein the electron tunneling (shortest) distance between two points (A and B) on neighboring CNFs consistently increases or decreases according to the predictions from the plane-strain transformation equation above (from B to B′) upon application of strain. Effectively, however, the net interparticle proximity increases in all cases shown due to particle rotation and uncurling. Conversely, arrangements yielding a strain-induced increase in interparticle separation are also possible. The unique spatial realignment associated with particle rotation and uncurling in the case of high-aspect-ratio particles promotes the apparent decrease in resistivity with increasing strain (negative piezoresistivity) at $\varepsilon < \varepsilon_c$. Other factors, such as the development of non-affine strain fields generated as a result of the large difference between the elastic moduli of the polymer matrix and the nanofibers, are also anticipated to influence the in-plane alignment of CNFs in the present CPN systems.

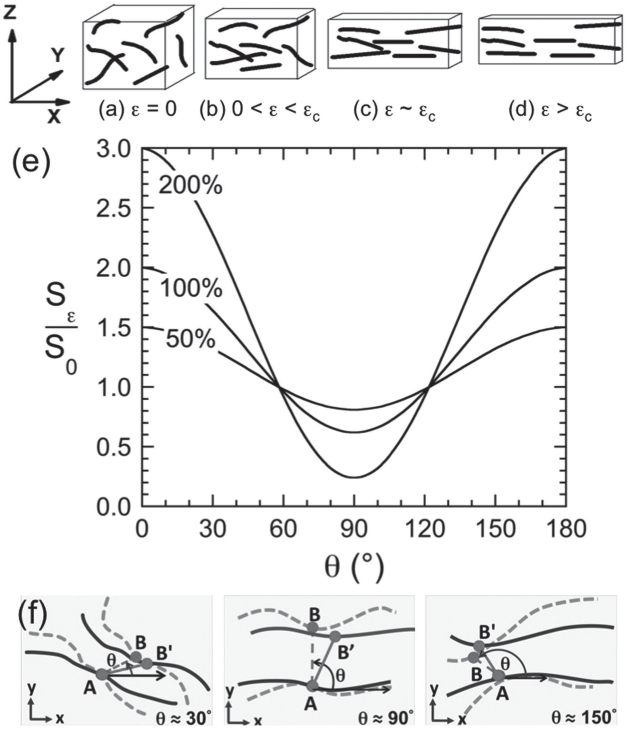

Figure 4. Schematic diagrams depicting the arrangement of high-aspect-ratio (nano)fibers responsible for strain-reversible piezoresistivity at different uniaxial strain stages: a) initially unstrained, b) at low strain levels below ε_c, c) at ε_c, and d) at high strain levels above ε_c. In (e), the normalized interparticle separation (S/S_0) is presented as a function of orientation angle (θ) for systems containing spherical particles, possessing a Poisson ratio (υ) of 0.4 and subjected to different uniaxial strain levels (labeled). Illustrations of the tunneling (shortest) distance between two points on (nano)fibers before (A to B, dashed lines) and after (A to B′, solid lines) application of uniaxial strain at different (approximate) orientation angles (labeled) are also included in (f).

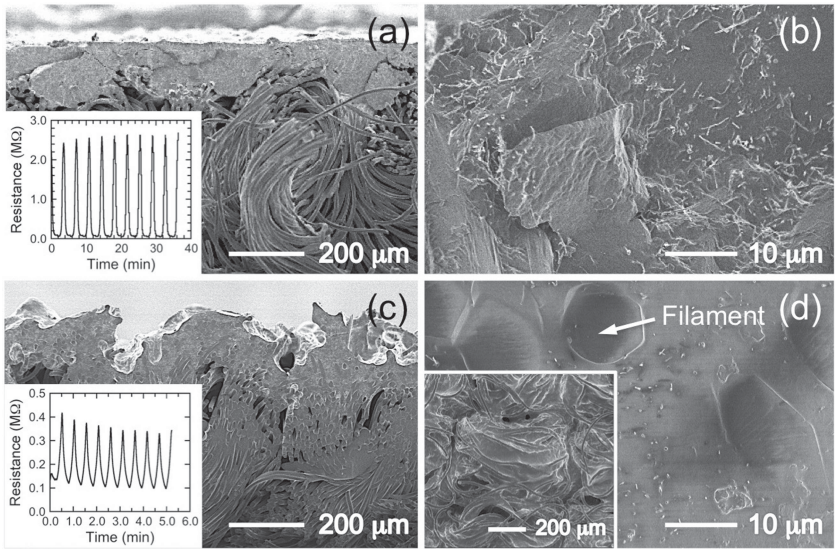

Figure 5. Series of cross-sectional SEM images differing in magnification and acquired from CPN coatings deposited on a knitted fabric representative of a commercial textile substrate: a,b) pPVC with 5 wt% CNF and 50 wt% DOS, and c,d) PDMS with 4 wt% CNF. The inset in (d) shows the surface of the PDMS-containing print layer, and the insets in (a,c) display the cyclical electrical resistance for print coatings subjected to maximum strain levels of 16% (a) and 10% (c).

2.3. Textile Sensory Behavior

As flexible strain sensors printed on textiles, the CPNs under investigation must exhibit sufficient sensitivity and adhesion to fabric substrates to warrant further consideration. The performance of a strain sensor is given in terms of its gauge factor (K), defined as $\Delta R/(\varepsilon R_0)$, where ΔR is the change from zero-strain resistance (R_0) due to an applied strain. Sensitivity increases with an increase in the magnitude of K. Linear plots of $\Delta R/R_0$ as a function of strain yield values of K that vary from −14.8 to −8.8 as φ is increased from 4 to 5 wt% CNF at 70% strain in PDMS-based CPNs. This increase in K with decreasing φ is most likely due to the proximity of φ to the percolation threshold. Equivalent values of K, broadly ranging from −19.6 to −42.6, are provided as functions of matrix composition and CNF content for the pPVC-based systems in Table 2. To put these values in perspective, the highest value of K reported[28] for a CPN sensor is 80, whereas values of 10–20 are not uncommon. Application of the present CPNs onto a fabric substrate results in the altered resistivity levels shown in Figure 1, but retention of the strain-reversible piezoresistivity and low-hysteresis cycling evident in Figure 2. The reason for the resistivity changes can be explained in terms of the print-layer morphologies, SEM images of which are displayed at different magnifications and orientations (cross-section versus surface) in **Figure 5** for both CPN series. Due to the significantly lower viscosity of the PDMS-based systems (7000 cP at 4 wt% CNF) compared to that of the pPVC-based materials (ca. 10^5 cP at 5 wt% CNF, selected to ensure ease of printability), the former penetrates into the fabric substrate and produces a macrocomposite containing voids, whereas the latter results in a distinctively smooth and contiguous coating on the fabric surface. Wicking of DOS from pPVC occurs as the coating is cured, however, and results in a reduction in interparticle contact resistance and, thus, higher conductivity (cf. Figure 1), as well as lower flexibility, relative to its free-standing film counterpart.

To ascertain the effectiveness of the present systems as fabric strain sensors, a prototype sleeve composed of a tight-fitting knitted fabric (70/30 w/w nylon/Spandex) coated with a pPVC-based CPN containing 5 wt% CNF and 50 wt% DOS and cured at 140 °C for 30 min (to form a surface layer measuring 550 μm thick) has been developed and tested by cyclical arm flexing (see the Supporting Information for a real-time movie clip).

3. Conclusions

Important highlights of this analysis include the following: the electrical response is highly repeatable, fully reversible, quickly recoverable (to its zero-strain resistance), and highly sensitive to small movements. This study establishes that CNF-containing CPNs, which are relatively inexpensive and facile to prepare, are capable of exhibiting strain-reversible piezoresistivity due to competition between in-plane alignment and longitudinal translation of high-aspect-ratio nanofibers, and that the critical strain delineating negative and positive piezoresistivity is sensitive to CPN composition and maximum strain amplitude upon cycling. These CPNs are sufficiently sensitive and robust for use as strain sensors to be printed on flexible substrates, thereby making them particularly attractive for electronic textiles, as well as other flexible electronic applications.

4. Experimental Section

Nanocomposite Preparation: The pPVC was prepared by blending PVC with a molecular weight of 50 kDa (Solvin 372 from Solvay America Inc., Houston, TX) with DOS, used as-received from Acros Organics (Fisher Scientific, Hampton, NH), and epoxidized soybean oil (ESO) from Spectrum Chemical Manufacturing Corp. (Gardena, CA) as a thermal stabilizer. A fabric bonding agent, designated Binder 2001, was obtained from Nazdar SourceOne (Greensboro, NC). The PDMS (Silastic BASE MDX4-4210, which contains silica) and the curing agent were purchased from Dow-Corning (Midland, MI). Reagent-grade *n*-hexane was procured from Fisher. Vapor-grown CNFs (VGCF-H), with a nominal diameter of 150 nm and lengths measuring up to 10–20 μm, were generously supplied by Showa Denko Corp. (Tokyo, Japan). For the pPVC-based CPNs, a calculated amount of DOS and 5 wt% ESO (relative to PVC) were combined for 10 s in a high-shear Mazerustar KK-50S mixer, after which time up to 14 wt% CNF was added and dispersed for 60 s. A corresponding amount of PVC in powder form was then included (to yield target PVC/DOS ratios) and mixed for an additional 60 s, followed by incorporation of 20 wt% binder (relative to PVC+DOS) and further mixing for 60 s.

Film Formation and Printing: The resultant paste was compression-molded at 140 °C for 30 min into films measuring 0.5 mm thick. The PDMS-based CPNs, on the other hand, were prepared by solvent casting.

After as much as 10 wt% CNF was dispersed by high-shear mixing in 25 mL *n*-hexane for 60 s, PDMS was added to the suspension and mixed for an additional 60 s before the curing agent (10 wt% relative to PDMS) was combined and mixed for 60 s. Curing was conducted at ambient temperature for 3 d to ensure complete cross-linking; the resulting films measured 0.7–0.8 mm thick. Selected to provide sufficient measurability and sensitivity, CPNs with either 5 wt% CNF (pPVC) or 4 wt% CNF (PDMS) were deposited on knitted fabrics measuring ca. 700 µm thick from Elastic Fabrics of America (Greensboro, NC) by screen-printing along the wale direction with a flat screen (mesh #60).

Characterization: Surface and cross-sectional SEM images of freestanding CPN films and fabric coatings were acquired on a JEOL 6400F field-emission microscope at operating voltages of 1 kV (pPVC) or 5 kV (PDMS). Electrical resistance was evaluated with a Keithley 6221/2182A meter using two- and four-point-probe methods, depending on the CNF concentration. Each measurement was acquired at nine different locations on a single specimen and averaged. Piezoresistive behavior was analyzed by inserting a specimen with four equispaced Cu leads (attached by Ag/Ni silicone adhesive) into a computer-controlled uniaxial load frame. Resistance was recorded as a function of time, and all CPNs in each series were evaluated for at least ten continuous loading/unloading cycles at a constant crosshead speed.

Supporting Information

Supporting Information is available from the Wiley Online Library or from the author.

Acknowledgements

This work was supported by the U.S. National Science Foundation. R.J.S. also expresses his gratitude for financial support from the Lars Onsager Professorship at NTNU.

Received: January 4, 2013
Revised: March 8, 2013
Published online: June 17, 2013

[1] R. Service, *Science* **2003**, *301*, 5635.
[2] B. O'Connor, K. H. An, Y. Zhao, K. P. Pipe, M. Shtein, *Adv. Mater.* **2007**, *19*, 22.
[3] T. Fujigaya, S. Haraguchi, T. Fukumaru, N. Nakashima, *Adv. Mater.* **2008**, *20*, 11.
[4] Y. H. Zhou, C. Fuentes-Hernandez, J. Shim, J. Meyer, A. J. Giordano, H. Li, P. Winget, T. Papadopoulos, H. Cheun, J. Kim, M. Fenoll, A. Dindar, W. Haske, E. Najafabadi, T. M. Khan, H. Sojoudi, S. Barlow, S. Graham, J. L. Bredas, S. R. Marder, A. Kahn, B. Kippelen, *Science* **2012**, *336*, 327.
[5] M. Hamedi, R. Forchheimer, O. Inganas, *Nat. Mater.* **2007**, *6*, 357.
[6] H. Okimoto, T. Takenobu, K. Yanagi, Y. Miyata, H. Shimotani, H. Kataura, Y. Iwasa, *Adv. Mater.* **2010**, *22*, 36.
[7] H. Minemawari, T. Yamada, H. Matsui, J. Tsutsumi, S. Haas, R. Chiba, R. Kumai, T. Hasegawa, *Nature* **2011**, *475*, 364.
[8] B. J. Munro, T. E. Campbell, G. G. Wallace, J. R. Steele, *Sens. Actuators B* **2008**, *131*, 2.
[9] B. B. Yue, C. Y. Wang, X. Ding, G. G. Wallace, *Electrochim. Acta* **2012**, *68*, 18.
[10] L. Jin, Z. Q. Feng, M. L. Zhu, T. Wang, M. K. Leach, Q. Jiang, *J. Biomed. Nanotechnol.* **2012**, *8*, 779.
[11] V. K. S. Shante, S. Kirkpatrick, *Adv. Phys.* **1971**, *20*, 325.
[12] F. Hussain, M. Hojjati, M. Okamoto, R. E. Gorga, *J. Compos. Mater.* **2006**, *40*, 1511.
[13] M. T. Byrne, Y. K. Gun'ko, *Adv. Mater.* **2010**, *22*, 15.
[14] X. Xie, Y. Mai, X. Zhou, *Mater. Sci. Eng. R* **2005**, *49*, 4.
[15] M.-J. Jiang, Z.-M. Dang, H.-P. Xu, *Appl. Phys. Lett.* **2007**, *90*, 042914.
[16] Q. Li, Y. Li, X. Zhang, S. B. Chikkannanavar, Y. Zhao, A. M. Dangelewicz, L. Zheng, S. K. Doorn, Q. Jia, D. E. Peterson, P. N. Arendt, Y. Zhu, *Adv. Mater.* **2007**, *19*, 20.
[17] N. Li, Y. Huang, F. Du, X. He, X. Lin, H. Gao, Y. Ma, F. Li, Y. Chen, P. Eklund, *Nano Lett.* **2006**, *6*, 6.
[18] S. Pfeifer, S.-H. Park, P. R. Bandaru, *J. Appl. Phys.* **2010**, *108*, 2.
[19] G. A. Jimenez, S. C. Jana, *Carbon* **2007**, *45*, 2079.
[20] A. Allaoui, S. V. Hoa, M. D. Pugh, *Compos. Sci. Technol.* **2008**, *68*, 2.
[21] M. H. Al-Saleh, U. Sundararaj, *Carbon* **2009**, *47*, 2.
[22] X. Fan, Z. Chu, F. Wang, C. Zhang, L. Chen, Y. Tang, D. Zou, *Adv. Mater.* **2008**, *20*, 3.
[23] M. Maccioni, E. Orgiu, P. Cosseddu, S. Locci, A. Bonfiglio, *Appl. Phys. Lett.* **2006**, *89*, 14.
[24] E. Scilingo, A. Gemignani, R. Paradiso, N. Taccini, B. Ghelarducci, D. de Rossi, *IEEE Trans. Inform. Technol. Biomed.* **2005**, *9*, 3.
[25] A. Tognetti, F. Lorussi, R. Bartalesi, S. Quaglini, M. Tesconi, G. Zupone, D. de Rossi, *J. Neuroeng. Rehab.* **2005**, *2*, 1.
[26] C. Huang, C. Shen, C. Tang, S. Chang, *Sens. Actuators A* **2008**, *141*, 2.
[27] X. W. Zhang, Y. Pan, Q. Zheng, X. S. Yi, *J. Polym. Sci. B* **2000**, *38*, 21.
[28] C. Cochrane, V. Koncar, M. Lewandowski, C. Dufour, *Sensors* **2007**, *7*, 473.
[29] C. Mattmann, F. Clemens, G. Tröster, *Sensors* **2008**, *8*, 3719.
[30] F. Lorussi, W. Rocchia, E. P. Scilingo, A. Tognetti, D. de Rossi, *IEEE Sens. J.* **2004**, *4*, 6.
[31] D. Stauffer, A. Aharony, *Introduction to Percolation Theory*, 2nd Ed., Taylor & Francis, London **1992.**
[32] I. Balberg, *Carbon* **2002**, *40*, 139.
[33] S. Vionnet-Menot, C. Grimaldi, T. Maeder, S. Strässler, P. Ryser, *Phys. Rev. B* **2005**, *71*, 064201.
[34] M.-J. Jiang, Z.-M. Dang, H.-P. Xu, *Appl. Phys. Lett.* **2006**, *89*, 182902.
[35] Z.-M. Dang, M.-J. Jiang, D. Xie, S.-H. Yao, L.-Q. Zhang, J. Bai, *J. Appl. Phys.* **2008**, *104*, 024114.
[36] S. El-Bouazzaoui, A. Droussi, M. E. Achour, C. Brosseau, *J. Appl. Phys.* **2009**, *106*, 104107.
[37] M. Ardanuy, M. A. Rodríguez-Perez, I. Algaba, *Compos. Part B - Eng.* **2011**, *42*, 4.
[38] B. I. Halperin, S. Feng, P. N. Sen, *Phys. Rev. Lett.* **1985**, *54*, 2391.
[39] S. Vionnet-Menot, C. Grimaldi, T. Maeder, S. Strassler, P. Ryser, *Phys. Rev. B* **2005**, *71*, 6.
[40] X. Zheng, M. G. Forest, R. Vaia, M. Arlen, R. Zhou, *Adv. Mater.* **2007**, *19*, 4038.
[41] Z. Chen, W. Ren, L. Gao, B. Liu, S. Pei, H. Cheng, *Nat. Mater.* **2011**, *10*, 6.
[42] Q. Fan, Z. Qin, S. Gao, Y. Wu, J. Pionteck, E. Mader, M. Zhu, *Carbon* **2012**, *50*, 4085.
[43] S. K. Kalanadhabhatla, *Ph.D. Dissertation*, North Carolina State University, Raleigh, NC **2012**.
[44] F. M. Du, J. E. Fischer, K. I. Winey, *Phys. Rev. B* **2005**, *72*, 121404.
[45] A. Behnam, J. Guo, A. Urala, *J. Appl. Phys.* **2007**, *102*, 044313.
[46] N. Pimparkar, C. Kocabas, S. J. Kang, J. Rogers, M. A. Alam, *IEEE Electr. Dev. Lett.* **2007**, *28*, 593.
[47] S. I. White, B. A. DiDonna, M. Mu, T. C. Lubensky, K. I. Winey, *Phys. Rev. B* **2009**, *79*, 024301.
[48] W. S. Bao, S. A. Meguid, Z. H. Zhu, M. J. Meguid, *Nanotechnology* **2011**, *22*, 485704.
[49] J. M. Gere, B. J. Goodno, *Mechanics of Materials*, 8th Ed., Cengage Learning, Stamford, CT **2013**.